Opuntia Ficus Indica based green composites for NPK fertilizer controlled release produced by compression molding and Fused Deposition Modeling

Roberto Scaffaro*, Maria Clara Citarrella, Emmanuel Fortunato Gulino

Department of Engineering, University of Palermo, Viale delle Scienze, ed. 6, 90128 Palermo, PA, Italy

* Corresponding author. Department of Engineering, University of Palermo, Viale delle Scienze, ed. 6, 90128 Palermo, PA, Italy.

Abstract

Excessive fertilization causes ecological problems due to leaching issues. To solve this problem and promote agriculture sustainability an innovative green composite for controlled release fertilizers was produced by adding NPK fertilizer flour to a biodegradable polymer with or without *Opuntia Ficus Indica* (OFI) particles. Six formulations were produced and employed for the fabrication of devices both for compression molding and fused deposition modeling (FDM). Both fillers displayed a good dispersion in the composites, excellent adhesion with the polymeric matrix and effectively acted as reinforcement. The decrease of NPK release rate (up to 30 days) was achieved using whole composites prepared. By appropriately selecting the dimension of the particles, the addition of OFI and the production technique, was possible to modulate the NPK release rate: FDM samples containing fine particles of OFI and NPK displayed the fastest release. Release data were fitted according to Peppas-Korsmeyer model to understand the release mechanism.

Keywords: Polymer-matrix composites (PMCs); Biocomposite; 3-D Printing; Compression moulding

1. Introduction

Recently, controlled release fertilizers (CRFs) are gaining increasing interest because of their crucial role in agriculture sustainability. Crops, in general, need nitrogen (N) to grow leaves, phosphorus (P) for roots, flowers and fruit growth and potassium (K) for the correct development of general functions of the plant. With the acronym NPK it is identified a class of fertilizers containing these three nutrients, commercially available in many compositions that are adapted to different considering crops requirements for a correct/fast growth.

Excessive fertilization causes ecological problems due to leaching issues. Moreover, the related economic wastages are also a problem that cannot be underestimated. CRFs devices may be able to release the nutrients continuously and regularly increasing their efficiency, reducing fertilizer loss, soil toxicity and frequency of the applications [1,2]. Encapsulating fertilizer in biodegradable polymeric matrices proved to be a possible strategy for producing composite materials with CRFs performance. Composite based on polyhydroxybutyrate (PHB) has been proposed for the production of devices for NPK controlled release. However, these composites exhibited an anomalous transport mechanism that

allow only a partial release of the loaded fertilizer during testing time (60 h). Moreover, PHB is considered as an expensive material [3,4]. Recently, a biodegradable nanocomposite polymeric device based on polyhydroxyalkanoate (PHA) was developed. This device exhibited a tunable degradability allowing to control phosphorus release and reducing its loss in the soil. Despite many benefits achieved, this device is not cost competitive [5].

Considering that, the actual goal is to produce CRFs devices that contextually are:

i) biodegradable [2–4,6];
ii) designed to provide tunable control of fertilizer release in order to be suitable to crops different life cycle or to environmental conditions of specific soils or climates [5];
iii) cost effective and easy to produce [1,3–5].

In this work, a possible strategy to overcome actual CRFs device limits and achieve the above described goal is proposed. More in detail, the approach adopted is using less expensive biodegradable polymers and combining them with biowaste, in order to decrease the amount of polymer needed. This route, in fact, could effective and drastically lower the cost of the final device Moreover, combining biodegradable polymers with natural fillers or agricultural waste allows enhancing mechanical performance [7–15], and contextually accelerating biodegradability [8,16].

Among all biopolymeric matrices polylactic acid (PLA), polycaprolactone (PCL), polybutylene adipate terephthalate (PBAT), cellulose and starch-based ones are the most commonly employed to obtain green composites [7,17,18]. Mater-Bi® (MB) is a family of biopolymers known for its interesting mechanical performance, good processability, thermal stability and biodegradability. Thanks to these interesting characteristics, MB, in recent years, has been used for different applications in which biodegradability is mandatory. Moreover, it widely proved to improve its mechanical performances when reinforced with natural fillers [7,8,19–21]. The addition of filler to a polymeric matrix, in general, resulting in a winning strategy in many others application fields [22–40].

Lands bordered by the Mediterranean Sea are rich in plants that could potentially be used (once they have been reduced to fiber or flours) for the production of biodegradable and bio-based polymeric composites. Among them, *Opuntia Ficus Indica* (OFI) flour proved to be an excellent option [9]. Its cladodes can be advantageously used in the production of green composites considering they constitute a very relevant agricultural scrap rich in a variety of constituents, including lignin and cellulose [41]. The addition of OFI flour to PLA, in fact, led to an increase in tensile properties on increasing filler content in composites produced by compression molding [9,41]. A winning strategy in order to reduce the environmental impact and the costs of CRF devices with adequate mechanical performance is to prepare composites based on a biodegradable matrix and biomass scraps [7].

Thermoplastic-based green composites are usually produced by extrusion, injection molding and compression molding (CM) [42]. Fused deposition modeling (FDM), however, has recently been investigated as an advantageous alternative for the production of green composites thanks to its possibility to create extremely elaborated geometries with a significant reduction of production time and costs [43–49]. These structures have been successfully employed in the pharmaceutical field for the production of drug release devices due to its potential to create complex and customized dosage forms [49–52]. In fact, by appropriately select process parameters such as infill and raster angle it is possible to tune the porosity of the devices and consequently them release kinetics [53–55]. Porosity, indeed, have a strong influence on drug/fertilizer delivery [56]. To the best of our knowledge, FDM was never used before to produce controlled release fertilizers devices. By using FDM, moreover, it is possible to easily and quickly create even articulated geometries with tunable porosity allowing to control the fertilizer release rate. These characteristics make FDM an attractive production technique for creating CRF devices based green composites.

The final goal of the present work was to produce CRFs devices by adding NPK flour to a biopolymeric matrix (Mater-Bi®) with or without OFI particles. For NPK and OFI flours two different granulometry (< 75 μm and 75–300 μm) were use and six formulations of biocomposites were produced and employed for the realization of CRF devices both for compression molding and FDM. Ultimately, the aim of this work is to control the release rate of NPK, chosen as model fertilizer compound, by embedding it on a compostable matrix and by exploring the possibility to tune the release from MB and MB/OFI composites by modifying flours granulometry and production techniques. To verify the achievement of this goal, release tests were performed and Peppas-Korsmeyer mathematical model was applied to modelize the obtained data.

2. Experimental section

2.1 Materials and Methods

2.1.1 Materials

The matrix used to prepare the composites was a sample of Mater-Bi® EF51L (MB), supplied by Novamont SpA (Novara, Italy) a polymer based on blends of aromatic and aliphatic biodegradable co-polyesters which composition is proprietary. Due to its composition, MB is moderately hygroscopic so, to avoid hydrolytic scissions during melt processing, it was vacuum-dried overnight at 60 °C. OFI cladodes, supplied by Bio Ecopuntia (Italy), were washed, ground, meshed and vacuum-dried overnight at 90 °C to remove any residual vegetation water. NPK 12-12-17 (supplied by Flortis, Orvital S.p.A.) was used as releasable fertilizer. It was vacuum-dried overnight at 40 °C to reduce potential MB chain scission phenomena during processing.

2.1.2 Preparation of composites

Firstly, OFI and NPK were separately grinded for 3 min and the obtained particles were sieved using different laboratory sieves (Controls, USA) selecting two different mesh sizes : under 75 μm (labeled as OFI-A and NPK-A) and from 75 μm to 300 μm (labeled as OFI-B and NPK-B). Particle size were selected to be suitable for the 3D printer preventing nozzle obstruction. In order to obtain a homogeneous dispersion of the filler, according to previous studies [7,9,44], the amount of filler to prepare hybrid biocomposites (ones containing both OFI and NPK) was chosen with the aim to not overcome total amount of filler of 20 wt.%. Six formulations namely MB/OFI-A, MB/OFI-B, MB/NPK-A, MB/NPK-B, MB/OFI-A/NPK-A and MB/OFI-B/NPK-B were produced by melt mixing. Hybrid composites, composites and pure MB, for comparison, were prepared by melt compounding in a Brabender internal mixer (T = 160 °C, rotor speed = 64 rpm, t = 5 min). The obtained blends were then extruded using a cylindrical nozzle (Haake Polylab single-screw extruder, Germany) with a thermal profile of 140-150-160-170 °C and a screw speed of 40 rpm. To obtain filaments suitable to be used for the 3D printer (diameter ~ 1.75 mm), the output extrudate were then drawn using a conveyor belt system set at a speed of 5.5 m/min.

Plaques for further characterization tests were obtained by compression molding using a laboratory press (Carver, Wabash, IN, USA) at 160 °C and 180 bar for 2 min. The samples (60 × 10 × 1 mm) obtained for fused deposition modeling (FDM) were prepared using Solid Edge 2019® and Simplify3D® software and printed using a Sharebot Next Generation (Italy) 3D printer. FDM processing parameters are reported in Table 1. After some trials, nozzle temperature of 160° was chosen aiming to achieve good printability avoiding nozzle obstructions. The other processing variables were selected considering previous works [44,57–59]. Other processing parameter were also chosen to promote NPK release and to optimize the mechanical performance [43,57]: infill rate 100%, rectilinear infill pattern, raster angle $\pm$ 45°. Code names of different produced samples together with their formulation are reported in Table 2 and some representative of them are shown in Figure 1.

2.2 Characterization

2.2.1 Morphological analysis

Morphological analysis of compression molded and FDM samples cross sections surfaces was performed before and after NPK release through Phenom ProX (Phenom-World, The Netherlands) scanning electron microscope (SEM) with electron magnification range of 80–130000x, optical magnification range of 20–135x, acceleration voltages of 15 kV and a maximal digital zoom of 12x. The samples were fractured in liquid nitrogen and then sputter-coated with a thin layer of gold (Sputtering Scancoat Six, Edwards) in order to avoid electrostatic discharge during the test. The samples were fixed on an aluminum stub appropriately designed for observing their cross sections.

2.2.2 Mechanical characterization

Mechanical performance of the samples was investigated by tensile tests by using an Instron 3365 machine (UK) in tensile mode and equipped with a 1kN load cell. The grip distance was set to 30 mm while two speeds were applied: 1 mm min^{-1} for 2 min and 50 mm min^{-1} until fracture occurred. The tests were performed on compression molded and FDM specimens (60 mm x 10 mm x 1 mm) before and after release tests, according to the ASTM D638 standard. Eight specimens were tested for each formulation and the outcomes of elastic modulus (E), tensile strength (TS), and elongation at break (EB), have been reported as average values ± standard deviations. Statistical analysis was performed on obtained data through unpaired Student *t*-test, using GraphPad Prism 9. Differences between two sets of data were considered statistically significant when the *p*-value obtained was lower than 0.05.

2.2.3 Water Contact Angle (WCA) Measurements

Surface wettability of biocomposites and pure matrices was determined through WCA testing (First Ten Angstroms FTA 1000, UK). An automatic liquid drop dosing system drips 4 μL of distilled water onto the samples and after 20 seconds images were taken. Five different spots of each sample were tested and WCA values have been reported as average values ± standard deviations. Statistical analysis was performed on obtained data through unpaired Student *t*-test, using GraphPad Prism 9. Differences between two sets of data were considered statistically significant when the *p*-value obtained was lower than 0.05.

2.2.4 Release of NPK fertilizer

NPK release from the composites was investigated at specific time intervals by submerging pre-weighed specimens (60 mm x 10 mm × 1 mm, 0.7 g) in 50 mL of DI water at 25 °C. All the samples were immersed in 50 ml of fresh DI water after each measurement. Electrolyte resistance of the obtained solution was evaluated through electrochemical impedance spectroscopy (EIS) using an AMETEK potentiostat/galvanostat (model PARSTAT 2273) and Power Suite software. To perform the measurements a three-electrode cell was used, equipped with a gold working electrode, a platinum plate applied as the counter electrode and a saturated Ag/AgCl as the reference electrode. EIS measurements were carried out at a frequency range from 100 kHz to 100 mHz, and potential amplitude of ±10 mV peak-to-peak versus open circuit potential (OCP). The electrolyte resistance (R) of solutions was then converted in conductivity (C) according to the equation:

$$C = \frac{1}{\rho} = \frac{R \cdot S}{l} \quad (1)$$

Where ρ is the resistivity, l is the length and S the cross-sectional area of the working electrode.

Control experiments were performed using free NPK (same amount present in composites) and biopolymeric matrix (without NPK). Each measurement was performed in triplicate.

Final conductivity value of free NPK was considered as 100% release and used as a standard for obtain the amount of NPK released from the devices.

2.2.5 Peppas-Korsmeyer model

The obtained release data were fitted according to the Peppas-Korsmeyer equation:

$$\frac{M_t}{M_\infty} = K\, t^n \quad (2)$$

Where M_t is the total amount of fertilizer released at time t, and M_∞ is the theoretical amount of NPK incorporated in the composites. By using Microsoft Office Excel software NPK release data were fitted according to equation (2) in order to determinate drug transport constants (K) and transport exponents (n) of the different formulations in the range of M_t/M_∞ 0–60% [60].

3. Result and discussion

3.1 Morphological analysis of OFI particles, NPK powder, green composites and CRF devices before NPK release

Morphology of OFI particles, NPK powder and obtained composites were analyzed by SEM. Relevant micrograph of natural organic filler and fertilizer in both mesh sizes (A and B) are shown in Figure 2. OFI and NPK particles showed a well distinguishable morphology. Even if both present inhomogeneity in shape and size, the natural filler displayed an elongated shape while the fertilizer is characterized by a more rounded form and a clear white color that makes it easily to identify. Morphological analysis was also performed on the cross section of composites and SEM micrographs of compression molded and FDM specimens are reported in Figure 3. It is possible to observe an almost homogeneous dispersion of filler and/or fertilizer in all samples. In addition, particles appear well embedded in the polymeric matrix and the adhesion between matrix and particles seem to be good for both OFI and NPK in both sizes (A and B). For FDM samples is possible to notice good adhesion between layers (see FDM samples micrograph in Figure 3 and Figure 4 a). The selected raster angle (± 45°), moreover, allowed to obtain a porous structure by creating separation points among adjacent raster layers (see FDM samples micrograph in Figure 3 and Figure 4 b).

3.2 Mechanical characterization of green composites and CRF devices before NPK release

Mechanical performance of samples was investigated by tensile tests. The values of elastic modulus (E), tensile strength (TS) and elongation at break (EB) of pure MB, MB composites (OFI or NPK) and MB hybrid composites (OFI and NPK) produced via compression molding and FDM are reported in Table 3. Regarding compression molded samples, CM_MB

shows a Young's modulus of 74.3 MPa a tensile strength of 19 MPa and an elongation-at-break of 821%. The addition of filler, fertilizer, or both in either mesh size (A and B), lead to an increase in E value (statistically significant, being $p < 0.0001$ for whole compositions, see Figure S1), a decrease in EB (statistically significant, being $p < 0.0001$ for whole compositions) while TS remained almost unchanged (not statistically significant, being $p > 0.05$). This behavior could be reasonably ascribed to the homogeneous dispersion of fillers and their good adhesion with the polymeric matrix (according to the morphological analysis). In particular, CM_MB/OFI-B showed a Young's modulus of 112 MPa and so an increase slightly higher if compared with CM_MB/OFI-A (98.1 MPa). On the contrary, no difference is observed between CM_MB/NPK-A and CM_MB/NPK-B. In fact, both showed a Young's modulus of ~ 95 MPa and an EB of ~ 64%. Hybrid composites (CM_MB/OFI-A/NPK-A and CM_MB/OFI-B/NPK-B) exhibited the highest increase in Young's modulus (~ 206%) and the lower value of elongation at break for the compression molded samples (~ 30%). This behavior could be reasonably explained considering that the total amount of fillers (i.e. OFI and NPK) for these latter is 20% being 10% in the previous cases. FDM composites and hybrid composites showed the same trend: the addition of filler, fertilizer, or both in either mesh size (A and B), lead to an increase in E value (statistically significant, being $p < 0.0001$ for whole compositions, see Figure S2). Moreover, the FDM prepared samples showed a slightly higher improvement of mechanical performance if compared to the ones obtained by compression molding (statistically significant, $p < 0.0001$ for whole compositions except for OFI-A and OFI-B/NPK-B series that showed $p = 0.067$ and $p = 0.08721$ respectively, see Figure S3). This behavior could be reasonably ascribed to 100% rectilinear infill [57,61] and the good adhesion between layers achieved during the printing process (according to morphological analysis). Mechanical property of FDM samples could be improved even more if a 0° raster angle had been selected [43]. On the contrary, an angle of ± 45° was selected in order to achieve in the composites a good compromise between optimization of tensile properties and promotion of NPK release due to its porous structure (see FDM samples micrograph in Figure 3 and Figure 4) that ± 45° raster angle allow to obtain.

3.3 Water Contact Angle (WCA) Measurements

In Figure 5 WCA of compression molded and FDM samples are reported. The addition of filler and / or fertilizer do not lead to a significative variation in surface wettability of the samples (statistically not significant, $p > 0.05$, see Figure S4). Contrariwise, all FDM samples showed a decrease in WCA value if compared with their compression molded counterpart (statistically significant, $p < 0.05$ for whole compositions, see Figure S5). This behavior could be reasonably ascribed to the pattern of the surface obtained with the selected raster angle. It is known in the scientific literature that wettability of FDM manufactured is affected by raster angle [62,63]. Moreover, despite results seems to not match Wenzel equation, is necessary to consider that the wetting behavior of composites obtained by FDM depends not only on surface roughness but also on pore morphology [63]. FDM samples, printed using ±45° raster angle, are characterized by interconnected

worm-like pores as could be noticed in Figure 6. According to Wenzel's equation, hydrophobicity is supposed to be further increased as roughness increases. However, it is known in the scientific literature that, despite surface roughness increases, the presence of long interconnected worm-like pores leads to an increase of hydrophilicity instead of hydrophobicity. The effect of porosity on wettability, in fact, overcome the one induced by surface roughness increases [64–66].

3.4 NPK release

Release profile of NPK from the samples was performed through conductivity measurements. Electrolyte resistance, in fact, can give information about the total concentration of electrolytes in solution. Electrolyte resistance was measured also for NPK (same content as in the composites) and for composites without NPK for control and results are shown in Figure 7a. The conductivity values for pure NPK reached rapidly a plateau region. In this case a complete release of the fertilizer is achieved in the first 24 hours of immersion. On the contrary, for all composites without NPK (CM_MB, CM_MB/OFI-A, CM_MB/OFI-B, FDM_MB, FDM_MB/OFI-A, FDM_MB/OFI-B) a low concentration of electrolytes was slowly and constantly released. The behavior of these latter could be reasonably attributable to some substances originate from the matrix and from the OFI which were released in water when the samples were submerged. It is necessary taking into account that this evaluation method overestimate the NPK release since in real condition, the NPK release occurs in soil and not in a liquid medium.

Conductivity tests of composites with NPK obtained by FDM and compression molding, carried out as a function of time in water at 25 °C, are shown in Figure 7b and 7c respectively. The NPK release kinetics of FDM composites (Figure 7b) is characterized, for all the specimens, by at least three phases: a burst release until 24 hours of immersion time, a second phase characterized by the progressive and slower release rate of NPK, and a final plateau region observed after 15 days of immersion. In detail, FDM_MB/OFI-A/NPK-A show a remarkable burst delivery with about 70% of NPK released in the first 24 hours. Other FDM composites showed a lower release of NPK, in particular, after 24 hours, FDM_MB/OFI-B/NPK-B released about 50% of NPK while FDM_MB/NPK-A and FDM_MB/NPK-B released about 40% and 45% respectively. This behavior could be reasonably be explained taking into account that, during immersion, OFI particles create channels along the polymeric matrix allowing the water to be conveyed inside the sample. This imply that NPK particles, present in the inner part of the samples, could be easier released. Moreover, as expected, the A series showed a faster release if compared with the respectively B counterparts for both normal and hybrid composites. A smaller particle size, in fact, allow a faster dissolution of the dispersed particles thanks to their greater exposed surface area. Compression molded specimen (Figure 7c) showed the same behavior of FDM ones but the compact structure of them significantly slow down the release of NPK. High porosities induced by FDM, in fact, significatively contribute to water transport

allowing the release of the NPK also from the more inner layer of the composites [67]. After 24 hours, in fact, CM_MB/OFI-A/NPK-A released about 25% of the fertilizer only.

The sustained release of NPK fertilizer, in general, was achieved using whole composites and hybrid composites prepared both from compression molding and FDM. All composites, in fact, if compared with free NPK, showed a significant reduction in conductivity, and so in the content of released compounds, especially in the first 24 hours. Moreover, appropriately selecting the dimension of the particles, the addition of OFI and the production technique it is possible to modulate the NPK release rate. More in detail, if a faster release is required CRFs devices should be prepare through FDM, OFI particles should be added to the polymeric matrix and NPK and OFI particles of 75 μm should be preferred. Moreover, this solution allows achieving a complete release of the fertilize. FDM_MB/OFI-A/NPK-A, in fact, act as the best CRF device considering its 100% release of NPK after 30 day. The total amount of NPK released for each composite at the end of the test, after 30 days, is resumed in Table 4. Compared with other CRFs reports in the literature, devices fabricated with this innovative method exhibited excellent ability to slow the release rate of NPK (see Table S1) [68–73].

3.5 Peppas-Korsmeyer model

Logarithmic plots of obtained NPK release data as a function of time (Figure 8) were evaluated to understand better the fertilizer release mechanism. On the firsts 5 hours of release test (Figure 8, region 1), the devices showed a burst release region in which reasonably the fertilizer available in composites surface is immediately delivered (first 30 min) and subsequently the delivery is driven by diffusive phenomena (Figure 8, region 2). After this first stage the slope of the release curves increases, likely due to the occurrence of some swelling phenomena across the polymeric matrix (Figure 8, region 3). This latter stage results more marked for FDM samples. The higher porosity induced by the process itself, in fact, reasonably lead to a relevant increase in water uptake and swelling for FDM structure if compared with the compact structure of compression molded devices [67]. After 24 hours, the fertilizer delivery is reasonably governed by both swelling and diffusive phenomena (Figure 8, region 4). Figure 9 provides a pictorial description of the release mechanism of the CRF composites.

In order to confirm these hypotheses on NPK release mechanism, the obtained release data were fit according to Peppas-Korsmeyer mathematical model [56,74,75]. Moreover, this model has previously been successfully used to describe fertilizer release kinetics from CRFs [6,76]. Value of K and n of the different formulations were determined and reported Table 5. Through n value is possible to obtain information about the release mechanism. In fact, when n is approximately 0.5, the fertilizer delivery is driven by diffusive phenomena; $n = 1$ indicates that release mechanism is governed by swelling and n values between 0.5 and 1 indicate an anomalous release, governed by swelling and diffusive phenomena [56,60,74]. However, the biopolymeric matrix may hinder diffusion, thus giving $n < 0.5$, while the presence of the

organic filler and the interconnected pore in FDM structure could provide the formation of internal channels in the samples allowing the release of the fertilizer incorporated in the innermost areas of the composite.

In particular, CM_MB/NPK-A (Figure 10a) showed a burst region that can be divided into two sub-regions, one characterized by faster kinetics ($n = 0.30$), probably attributable to some NPK particles available in the composite surface and thus faster delivered, and a second region that provide information about the actual capability of the system to establish a controlled release ($n = 0.16$). However, in both regions $n < 0.5$, especially in the second region, therefore the composite could indeed slow the fertilizer release. CM_MB/OFI-A/NPK-A (Figure 10b) showed the same scenario but with a first region characterized by a much faster kinetics ($n = 0.75$). This behavior could be reasonably imputable to the presence of OFI particles in the matrix as already discussed. CM_MB/NPK-B and CM_MB/OFI-B/NPK-B (Figure 10c), instead, showed a single region characterize by a hinder diffusion of the NPK ($n = 0.25$ and $n = 0.35$), ensuring an almost Fickian release mechanism. Likewise, FDM_MB/NPK-A and FDM_MB/OFI-A/NPK-A (Figure 10d) showed a hinder diffusion of fertilizer with n value of 0.24 and 0.34 respectively. On the contrary, FDM_MB/NPK-B (Figure 10e) and FDM_MB/OFI-B/NPK-B (Figure 10f) showed two sub-regions, one characterized by faster kinetics, especially for FDM_MB/NPK-B ($n = 0.74$), and the second that confirm the capability of the systems to establish a controlled release ($n = 0.27$ and $n = 0.21$ respectively). In general, all composites showed a significant hinder diffusion of the NPK, especially in the first 24 hours, that can be modulated by appropriately selecting the dimension of the particles of the fertilizer, the addition of OFI and the production technique. The obtained CRFs composites ensuring an almost Fickian release mechanism, unlike NPK grain, where NPK is immediately released because of its instantaneous dissolution.

3.6 Morphological analysis of CRF devices after NPK release

Morphology of CRF were analyzed also after NPK release (30 days of soaking in distilled water) and relevant SEM micrograph of them are showed in Figure 11. It is possible to notice that all CRF devices displayed an evident degradation of the polymeric matrix. Moreover, all the composites showed voids in the matrix (not detectable in the samples before the release) reasonably produced by the dissolution of released NPK. Some NPK particle are still present in all device except FDM_MB/OFI-A/NPK-A. In this latter, in fact, no particles of fertilizer can be detected confirming the 100% NPK release. Furthermore, optical image (Figure 12a) and micrograph of the FDM samples before (Figure 12b) and after (Figure 12c) the release were reported. In Figure 12b it is possible to notice the good adhesion of adjacent layer in FDM samples before NPK release. After soaking in water for 30 days, instead, the samples showed a detachment of the layers (Figure 12c). This behavior testifies the occurrence of swelling of the polymeric matrix confirming the supposed mechanism of release.

3.7 Mechanical characterization of CRF devices after NPK release

Mechanical performance of samples after 30 days of NPK release was investigated by tensile tests and the values of elastic modulus (E), tensile strength (TS) and elongation at break (EB) are reported in Table 6. Samples without NPK were also immersed in DI water for 30 days and then tested for comparison. Regarding compression molded samples, all the specimen without NPK (CM_MB, CM_MB/OFI-A, CM_MB/OFI-B) showed an increase in Young's modulus (statistically significant, being $p < 0.05$, see Figure S6) reasonably imputable to the degradation of the biopolymeric matrix [77]. Concerning CM_MB/NPK-A and CM_MB/NPK-B, no difference in E can be observed before and after the fertilizer release (variation not statistically significant, being $p > 0.05$, see Figure S6), in fact, both showed a Young's modulus of ~ 95 MPa. This behavior could be read as the result of the decrease of E due to the filler (NPK) loss during the release phase and a simultaneous increase of it imputable to the degradation of the matrix. On the contrary, hybrid composites (CM_MB/OFI-A/NPK-A and CM_MB/OFI-B/NPK-B) exhibited a slight decrease in Young's modulus (statistically significant, being $p < 0.05$, see Figure S6). In this case, the effect of the filler loss during the release phase predominate on the biodegradation effect considering that the total amount of filler for these latter is 20% and no more 10%. Moreover, the weakening of filler/matrix interfacial interactions due to water and the poorer filler properties due to a plasticizing effect could affect on mechanical performance inducing a reduction in stiffness [67].

Concerning FDM sample it is also necessary to take into account that the high porosities induced by the process, not only promote the water transport across the samples allowing the release of the NPK also from the more inner layer of the composites but also leads to a relevant increase of water uptake and swelling if compared to compression molded samples [67]. FDM_MB, in fact, showed a slight decrease in E value (statistically significant, being $p < 0.05$, see Figure S6) probably imputable to its hygroscopic behavior. This decrease was even more marked in OFI and / or NPK containing samples were also the effect of filler loss during the release phase should be considered. In detail, FDM_MB/OFI-A and FDM_MB/OFI-B displayed a decrease in Young's modulus from 113 to 101 MPa and from 128 to 114 MPa respectively (statistically significant, being $p < 0.05$, see Figure S6). When only NPK is added to the biopolymeric matrix (FDM_MB/NPK-A and FDM_MB/NPK-B) the decrease in E value is more marked (statistically significant, being $p < 0.05$, see Figure S6). This behavior could be reasonably imputable to the higher filler loss due to the better solubility of NPK if compared with OFI one. Moreover, FDM_MB/OFI-A/NPK-A and FDM_MB/OFI-B/NPK-B showed the highest decrease in Young's modulus value (statistically significant, being $p < 0.05$, see Figure S6) due to the even higher filler loss that occurs for these samples. Should be considered, in fact, that the total amount of filler for these latter is 20% and no more 10% (since 10% of OFI and 10% of NPK is present).

Conclusions

An innovative green composite with CRFs performance was produced by adding NPK flour to a biodegradable polymer (Mater-Bi®) with or without OFI particles. The final devices were successfully fabricated both for compression molding and FDM using all the prepared formulation. Both filler and fertilizer displayed good dispersion in the composites, excellent adhesion with the polymeric matrix and effectively acted as reinforcement. FDM samples, moreover, showed higher mechanical properties if compared with compression molded ones. Release tests of CRF devices reveal the ability of all the obtained composites to slow the release rate of NPK (up to 30 days), which proved to be tunable by modifying formulation, flours granulometry and production techniques. The porous structure of FDM samples, induced by the process itself, promote the water transport across the devices allowing the release of the NPK also from the more inner layer. In particular, FDM_MB/OFI-A/NPK-A act as the best CRF device showing a remarkable burst delivery with about 70% of NPK released in the first 24 hours and a 100% release after 30 days. Compression molded specimens showed the same behavior of FDM ones but the compact structure of them significantly slow down the release of NPK. Considering release kinetics results, it is possible to conclude that by adding filler, varying fertilizer and filler granulometry and by employing different production technique it is possible to tune NPK release in order to be suitable to crops different life cycle or to environmental conditions of specific soils or climates. More in detail, by addig OFI particles to the polymeric matrix and select 75 μm NPK and OFI particles it is possible to obtain CRFs devices characterized by a faster release. Biodegradable, cost effective and easy to produce CRF green composites could be prepared through FDM by adding NPK and OFI flours to a biodegradable polymeric matrix. The addition of OFI, in fact, leads to a decrease of the amount of polymer needed and consequently to a lowering in the cost of the final device. Moreover, by using FDM it is possible to reduce production time and costs, create extremely elaborated geometries as well as easy tune the NPK release rate.

References

[1] Vejan P, Khadiran T, Abdullah R, Ahmad N. Controlled release fertilizer: A review on developments, applications and potential in agriculture. Journal of Controlled Release 2021;339:321–34. https://doi.org/10.1016/j.jconrel.2021.10.003.

[2] Jarosiewicz A, Tomaszewska M. Controlled-release NPK fertilizer encapsulated by polymeric membranes. Journal of Agricultural and Food Chemistry 2003;51:413–7. https://doi.org/10.1021/jf020800o.

[3] Souza J de L, Chiaregato CG, Faez R. Green Composite Based on PHB and Montmorillonite for KNO3 and NPK Delivery System. Journal of Polymers and the Environment 2018;26:670–9. https://doi.org/10.1007/s10924-017-0979-4.

[4] Souza JL, de Campos A, França D, Faez R. PHB and Montmorillonite Clay Composites as KNO3 and NPK Support for a Controlled Release. Journal of Polymers and the Environment 2019;27:2089–97. https://doi.org/10.1007/S10924-019-01498-9/TABLES/2.

[5] Sigmon LR, Adisa IO, Liu B, Elmer WH, White JC, Dimkpa CO, et al. Biodegradable Polymer Nanocomposites Provide Effective Delivery and Reduce Phosphorus Loss during Plant Growth. ACS Agricultural Science and Technology 2021. https://doi.org/10.1021/acsagscitech.1c00149.

[6] Noppakundilograt S, Pheatcharat N, Kiatkamjornwong S. Multilayer-coated NPK compound fertilizer hydrogel with controlled nutrient release and water absorbency. Journal of Applied Polymer Science 2015;132. https://doi.org/10.1002/app.41249.

[7] Scaffaro R, Citarrella MC, Gulino EF, Morreale M. Hedysarum coronarium-Based Green Composites Prepared by Compression Molding and Fused Deposition Modeling. Materials 2022;15. https://doi.org/10.3390/ma15020465.

[8] Bordón P, Paz R, Peñalva C, Vega G, Monzón M, García L. Biodegradable polymer compounds reinforced with banana fiber for the production of protective bags for banana fruits in the context of circular economy. Agronomy 2021;11. https://doi.org/10.3390/agronomy11020242.

[9] Scaffaro R, Maio A, Gulino EF, Megna B. Structure-property relationship of PLA-Opuntia Ficus Indica biocomposites. Composites Part B: Engineering 2019;167:199–206. https://doi.org/10.1016/j.compositesb.2018.12.025.

[10] Scaffaro R, Lopresti F, Botta L. PLA based biocomposites reinforced with Posidonia oceanica leaves. Composites Part B: Engineering 2018;139:1–11. https://doi.org/10.1016/j.compositesb.2017.11.048.

[11] Benito-González I, López-Rubio A, Martínez-Sanz M. Potential of lignocellulosic fractions from Posidonia oceanica to improve barrier and mechanical properties of bio-based packaging materials. International Journal of Biological Macromolecules 2018;118:542–51. https://doi.org/10.1016/j.ijbiomac.2018.06.052.

[12] Boudjema HL, Bendaikha H, Maschke U. Green composites based on Atriplex halimus fibers and PLA matrix. Journal of Polymer Engineering 2020;40:693–702. https://doi.org/10.1515/polyeng-2020-0068.

[13] Scaffaro R, Gulino EF, Citarrella MC, Maio A. Green Composites Based on Hedysarum coronarium with Outstanding FDM Printability and Mechanical Performance. Polymers 2022, Vol 14, Page 1198 2022;14:1198. https://doi.org/10.3390/POLYM14061198.

[14] Culebras M, Collins GA, Beaucamp A, Geaney H, Collins MN. Lignin/Si Hybrid Carbon Nanofibers towards Highly Efficient Sustainable Li-ion Anode Materials. Engineered Science 2022;17:195–203. https://doi.org/10.30919/ES8D608.

[15] Al-Harbi N, Hussein MA, Al-Hadeethi Y, Umar A. Cellulose Acetate-Hydroxyapatite-Bioglass-Zirconia Nanocomposite Particles as Potential Biomaterial: Synthesis, Characterization, and Biological Properties for Bone Application. Engineered Science 2022;17:70–82. https://doi.org/10.30919/ES8D528.

[16] Scaffaro R, Maio A, Gulino EF. Hydrolytic degradation of PLA/Posidonia Oceanica green composites: A simple model based on starting morpho-chemical properties. Composites Science and Technology 2021;213:108930. https://doi.org/10.1016/j.compscitech.2021.108930.

[17] Tejyan S, Baliyan NK, Patel VK, Patnaik A, Singh T. Polymer green composites reinforced with natural fibers: A comparative study. Materials Today: Proceedings 2020;44:4767–9. https://doi.org/10.1016/j.matpr.2020.10.971.

[18] Rafiee K, Schritt H, Pleissner D, Kaur G, Brar SK. Biodegradable green composites: It's never too late to mend. Current Opinion in Green and Sustainable Chemistry 2021;30:100482. https://doi.org/10.1016/j.cogsc.2021.100482.

[19] Re G lo, Morreale M, Scaffaro R, la Mantia FP. Biodegradation paths of Mater-Bi®/kenaf biodegradable composites. Journal of Applied Polymer Science 2013;129:3198–208. https://doi.org/10.1002/app.39027.

[20] Morreale M, Scaffaro R, Maio A, la Mantia FP. Mechanical behaviour of Mater-Bi®/wood flour composites: A statistical approach. Composites Part A: Applied Science and Manufacturing 2008;39:1537–46. https://doi.org/10.1016/j.compositesa.2008.05.015.

[21] Scaffaro R, Maio A, Lopresti F. Physical properties of green composites based on poly-lactic acid or Mater-Bi® filled with Posidonia Oceanica leaves. Composites Part A: Applied Science and Manufacturing 2018;112:315–27. https://doi.org/10.1016/j.compositesa.2018.06.024.

[22] Vijeata A, Chaudhary GR, Umar A, Chaudhary S. Distinctive solvatochromic response of fluorescent carbon dots derived from different components of aegle marmelos plant. Engineered Science 2021;15:197–209. https://doi.org/10.30919/ES8E512.

[23] Thota SP, Bag PP, Vadlani PV, Belliraj SK. Plant Biomass Derived Multidimensional Nanostructured Materials: A Green Alternative for Energy Storage. Engineered Science 2022. https://doi.org/10.30919/ES8D664.

[24] Stephen C, Shivamurthy B, Mohan M, Mourad A-HI, Selvam R, Thimmappa BHS. Low Velocity Impact Behavior of Fabric Reinforced Polymer Composites– A Review. Engineered Science 2022. https://doi.org/10.30919/ES8D670.

[25] Shahabaz SM, Sharma S, Shetty N, Shetty SD, Gowrishankar MC. Influence of Temperature on Mechanical Properties and Machining of Fibre Reinforced Polymer Composites: A Review. Engineered Science 2021;16:26–46. https://doi.org/10.30919/ES8D553.

[26] More AP. Flax fiber–based polymer composites: a review. Advanced Composites and Hybrid Materials 2022;5:1–20. https://doi.org/10.1007/S42114-021-00246-9/FIGURES/7.

[27] Vinod B, Suresh S, Sudhakara D. Investigation of biodegradable hybrid composites: effect of fibers on tribo-mechanical characteristics. Advanced Composites and Hybrid Materials 2020;3:194–204. https://doi.org/10.1007/S42114-020-00148-2/FIGURES/7.

[28] Gupta US, Dhamarikar M, Dharkar A, Tiwari S, Namdeo R. Study on the effects of fibre volume percentage on banana-reinforced epoxy composite by finite element method. Advanced Composites and Hybrid Materials 2020;3:530–40. https://doi.org/10.1007/S42114-020-00179-9/FIGURES/15.

[29] Kivade SB, Gunge A, Nagamadhu M, Rajole S. Mechanical and dynamic mechanical behavior of acetylation-treated plain woven banana reinforced biodegradable composites. Advanced Composites and Hybrid Materials 2022;5:144–58. https://doi.org/10.1007/S42114-021-00247-8/FIGURES/20.

[30] Wu H, Zhong Y, Tang Y, Huang Y, Liu G, Sun W, et al. Precise regulation of weakly negative permittivity in CaCu3Ti4O12 metacomposites by synergistic effects of carbon nanotubes and grapheme. Advanced Composites and Hybrid Materials 2022;5:419–30. https://doi.org/10.1007/S42114-021-00378-Y/FIGURES/5.

[31] Qi G, Liu Y, Chen L, Xie P, Pan D, Shi Z, et al. Lightweight Fe3C@Fe/C nanocomposites derived from wasted cornstalks with high-efficiency microwave absorption and ultrathin thickness. Advanced Composites and Hybrid Materials 2021;4:1226–38. https://doi.org/10.1007/S42114-021-00368-0/FIGURES/8.

[32] Xie P, Liu Y, Feng M, Niu M, Liu C, Wu N, et al. Hierarchically porous Co/C nanocomposites for ultralight high-performance microwave absorption. Advanced Composites and Hybrid Materials 2021;4:173–85. https://doi.org/10.1007/S42114-020-00202-Z/FIGURES/9.

[33] Xie P, Zhang Z, Wang Z, Sun K, Fan R. Targeted Double Negative Properties in Silver/Silica Random Metamaterials by Precise Control of Microstructures. Research 2019;2019:1–11. https://doi.org/10.34133/2019/1021368.

[34] Wu H, Sun H, Han F, Xie P, Zhong Y, Quan B, et al. Negative Permittivity Behavior in Flexible Carbon Nanofibers-Polydimethylsiloxane Films. Engineered Science 2022;17:113–20. https://doi.org/10.30919/ES8D576.

[35] Kivade SB, Gunge A, Nagamadhu M, Rajole S. Mechanical and dynamic mechanical behavior of acetylation-treated plain woven banana reinforced biodegradable composites. Advanced Composites and Hybrid Materials 2022;5:144–58. https://doi.org/10.1007/S42114-021-00247-8/FIGURES/20.

[36] Wu K, Liu Y, Ma Y, Tan M, Chai T, Hu F, et al. Pretreatment of hydroxy-terminated polybutadiene (HTPB)/toluene diisocyanate (TDI) binder system for biodegradation. Advanced Composites and Hybrid Materials 2021;4:96–103. https://doi.org/10.1007/S42114-020-00197-7/FIGURES/7.

[37] Dhatarwal P, Sengwa RJ. Structural and dielectric characterization of (PVP/PEO)/Al2O3 nanocomposites for biodegradable nanodielectric applications. Advanced Composites and Hybrid Materials 2020;3:344–53. https://doi.org/10.1007/S42114-020-00168-Y/FIGURES/6.

[38] Mokhtari S, Yekta BE, Marghussian V, Pooya &, Ahmadi T. Synthesis and characterization of biodegradable AZ31/calcium phosphate glass composites for orthopedic applications. Advanced Composites and Hybrid Materials 2020 3:3 2020;3:390–401. https://doi.org/10.1007/S42114-020-00177-X.

[39] Yu Z, Yan Z, Zhang F, Wang J, Shao Q, Murugadoss V, et al. Waterborne acrylic resin co-modified by itaconic acid and γ-methacryloxypropyl triisopropoxidesilane for improved mechanical properties, thermal stability, and corrosion resistance. Progress in Organic Coatings 2022;168:106875. https://doi.org/10.1016/J.PORGCOAT.2022.106875.

[40] Jing X, Li Y, Zhu J, Chang L, Maganti S, Naik N, et al. Improving thermal conductivity of polyethylene/polypropylene by styrene-ethylene-propylene-styrene wrapping hexagonal boron nitride at the phase interface. Advanced Composites and Hybrid Materials 2022;1:1–10. https://doi.org/10.1007/S42114-022-00438-X/FIGURES/5.

[41] Greco A, Gennaro R, Timo A, Bonfantini F, Maffezzoli A. A Comparative Study Between Bio-composites Obtained with Opuntia ficus indica Cladodes and Flax Fibers. Journal of Polymers and the Environment 2013;21:910–6. https://doi.org/10.1007/s10924-013-0595-x.

[42] Gholampour A, Ozbakkaloglu T. A review of natural fiber composites: properties, modification and processing techniques, characterization, applications. vol. 55. Springer US; 2020. https://doi.org/10.1007/s10853-019-03990-y.

[43] Rajendran Royan NR, Leong JS, Chan WN, Tan JR, Shamsuddin ZSB. Current state and challenges of natural fibre-reinforced polymer composites as feeder in fdm-based 3d printing. Polymers (Basel) 2021;13. https://doi.org/10.3390/polym13142289.

[44] Scaffaro R, Maio A, Gulino EF, Alaimo G, Morreale M. Green composites based on pla and agricultural or marine waste prepared by fdm. Polymers (Basel) 2021;13:1–17. https://doi.org/10.3390/polym13091361.

[45] Liu Z, Lei Q, Xing S. Mechanical characteristics of wood, ceramic, metal and carbon fiber-based PLA composites fabricated by FDM. Journal of Materials Research and Technology 2019;8:3743–53. https://doi.org/10.1016/j.jmrt.2019.06.034.

[46] Mohamed OA, Masood SH, Bhowmik JL. Experimental Investigations of Process Parameters Influence on Rheological Behavior and Dynamic Mechanical Properties of FDM Manufactured Parts. Materials and Manufacturing Processes 2016;31:1983–94. https://doi.org/10.1080/10426914.2015.1127955.

[47] Kopparthy SDS, Netravali AN. Review: Green composites for structural applications. Composites Part C: Open Access 2021;6:100169. https://doi.org/10.1016/j.jcomc.2021.100169.

[48] Mazzanti V, Malagutti L, Mollica F. FDM 3D printing of polymers containing natural fillers: A review of their mechanical properties. Polymers (Basel) 2019;11. https://doi.org/10.3390/polym11071094.

[49] Dumpa N, Butreddy A, Wang H, Komanduri N, Bandari S, Repka MA. 3D printing in personalized drug delivery: An overview of hot-melt extrusion-based fused deposition modeling. International Journal of Pharmaceutics 2021;600:120501. https://doi.org/10.1016/J.IJPHARM.2021.120501.

[50] Cailleaux S, Sanchez-Ballester NM, Gueche YA, Bataille B, Soulairol I. Fused Deposition Modeling (FDM), the new asset for the production of tailored medicines. Journal of Controlled Release 2021;330:821–41. https://doi.org/10.1016/J.JCONREL.2020.10.056.

[51] Goyanes A, Wang J, Buanz A, Martínez-Pacheco R, Telford R, Gaisford S, et al. 3D Printing of Medicines: Engineering Novel Oral Devices with Unique Design and Drug Release Characteristics. Molecular Pharmaceutics 2015;12:4077–84. https://doi.org/10.1021/ACS.MOLPHARMACEUT.5B00510/ASSET/IMAGES/ACS.MOLPHARMACEUT.5B00510.SOCIAL.JPEG_V03.

[52] Alhijjaj M, Belton P, Qi S. An investigation into the use of polymer blends to improve the printability of and regulate drug release from pharmaceutical solid dispersions prepared via fused deposition modeling (FDM) 3D printing. European Journal of Pharmaceutics and Biopharmaceutics 2016;108:111–25. https://doi.org/10.1016/J.EJPB.2016.08.016.

[53] Goyanes A, Fina F, Martorana A, Sedough D, Gaisford S, Basit AW. Development of modified release 3D printed tablets (printlets) with pharmaceutical excipients using additive manufacturing. International Journal of Pharmaceutics 2017;527:21–30. https://doi.org/10.1016/J.IJPHARM.2017.05.021.

[54] Palekar S, Nukala PK, Mishra SM, Kipping T, Patel K. Application of 3D printing technology and quality by design approach for development of age-appropriate pediatric formulation of baclofen. International Journal of Pharmaceutics 2019;556:106–16. https://doi.org/10.1016/J.IJPHARM.2018.11.062.

[55] Goyanes A, Robles Martinez P, Buanz A, Basit AW, Gaisford S. Effect of geometry on drug release from 3D printed tablets. International Journal of Pharmaceutics 2015;494:657–63. https://doi.org/10.1016/J.IJPHARM.2015.04.069.

[56] Gulino EF, Citarrella MC, Maio A. An innovative route to prepare in situ graded crosslinked PVA graphene electrospun mats for drug release. Composites Part A 2022:106827. https://doi.org/10.1016/j.compositesa.2022.106827.

[57] Alvarez C. KL, Lagos C. RF, Aizpun M. Investigating the influence of infill percentage on the mechanical properties of fused deposition modelled ABS parts. Ingenieria e Investigacion 2016;36:110–6. https://doi.org/10.15446/ing.investig.v36n3.56610.

[58] Mahmood S, Qureshi AJ, Goh KL, Talamona D. Tensile strength of partially filled FFF printed parts: Experimental results. Rapid Prototyping Journal 2017;23:122–8. https://doi.org/10.1108/RPJ-08-2015-0115.

[59] Dave HK, Patadiya NH, Prajapati AR, Rajpurohit SR. Effect of infill pattern and infill density at varying part orientation on tensile properties of fused deposition modeling-printed poly-lactic acid part. Proceedings of the Institution of Mechanical Engineers, Part C: Journal of Mechanical Engineering Science 2021;235:1811–27. https://doi.org/10.1177/0954406219856383.

[60] Ritger PL, Peppas NA. A simple equation for description of solute release II. Fickian and anomalous release from swellable devices. Journal of Controlled Release 1987;5:37–42. https://doi.org/10.1016/0168-3659(87)90035-6.

[61] Rajendran Royan NR, Leong JS, Chan WN, Tan JR, Shamsuddin ZSB. Current state and challenges of natural fibre-reinforced polymer composites as feeder in fdm-based 3d printing. Polymers (Basel) 2021;13. https://doi.org/10.3390/polym13142289.

[62] Haryńska A, Carayon I, Kosmela P, Szeliski K, Łapiński M, Pokrywczyńska M, et al. A comprehensive evaluation of flexible FDM/FFF 3D printing filament as a potential material in medical application. European Polymer Journal 2020;138:109958. https://doi.org/10.1016/j.eurpolymj.2020.109958.

[63] Modi U, Prakash S. Wettability of 3D printed polylactic acid (PLA) parts. AIP Conference Proceedings 2019;2148. https://doi.org/10.1063/1.5123974.

[64] Mehrvarz A, Khalil-Allafi J, Khosrowshahi AK. Biocompatibility and antibacterial behavior of electrochemically deposited Hydroxyapatite/ZnO porous nanocomposite on NiTi biomedical alloy. Ceramics International 2022. https://doi.org/10.1016/J.CERAMINT.2022.02.183.

[65] Xiong B, Li J, He C, Tang X, Lv Z, Li X, et al. Effect of pore morphology and surface roughness on wettability of porous titania films. Materials Research Express 2020;7:115013. https://doi.org/10.1088/2053-1591/abc770.

[66] Mehrvarz A, Khalil-Allafi J, Etminanfar M, Mahdavi S. The study of morphological evolution, biocorrosion resistance, and bioactivity of pulse electrochemically deposited Hydroxyapatite/ZnO composite on NiTi superelastic alloy. Surface and Coatings Technology 2021;423:127628. https://doi.org/10.1016/J.SURFCOAT.2021.127628.

[67] le Duigou A, Castro M, Bevan R, Martin N. 3D printing of wood fibre biocomposites: From mechanical to actuation functionality. Materials and Design 2016;96:106–14. https://doi.org/10.1016/j.matdes.2016.02.018.

[68] Lubkowski K, Smorowska A, Sawicka M, Wróblewska E, Dzienisz A, Kowalska M, et al. Ethylcellulose as a coating material in controlled-release fertilizers. Polish Journal of Chemical Technology 2019;21:52–8. https://doi.org/10.2478/PJCT-2019-0010.

[69] Messa LL, Faez R. Spray-dried chitosan/nanocellulose microparticles: synergistic effects for the sustained release of NPK fertilizer. Cellulose 2020;27:10077–93. https://doi.org/10.1007/S10570-020-03482-2/FIGURES/9.

[70] Olad A, Zebhi H, Salari D, Mirmohseni A, Reyhani Tabar A. Slow-release NPK fertilizer encapsulated by carboxymethyl cellulose-based nanocomposite with the function of water retention in soil. Materials Science and Engineering: C 2018;90:333–40. https://doi.org/10.1016/J.MSEC.2018.04.083.

[71] Baki M, Abedi-Koupai J. Preparation and characterization of a superabsorbent slow-release fertilizer with sodium alginate and biochar. Journal of Applied Polymer Science 2018;135:45966. https://doi.org/10.1002/APP.45966.

[72] Rozo G, Bohorques L, Santamaría J. Controlled release fertilizer encapsulated by a κ-carrageenan hydrogel. Polimeros 2019;29. https://doi.org/10.1590/0104-1428.02719.

[73] de GUZMAN J, dela Peña K, Ytac Dorothy J, Tumolva T. Synthesis and Characterization of Ionically-Crosslinked κ- Carrageenan/Sodium Alginate/Carboxymethyl Cellulose Hydrogel Blends for Soil Water Retention and Fertilizer Release. Solid State Phenomena 2020;304:59–65. https://doi.org/10.4028/WWW.SCIENTIFIC.NET/SSP.304.59.

[74] Costa P, Sousa Lobo JM. Modeling and comparison of dissolution profiles. European Journal of Pharmaceutical Sciences 2001;13:123–33. https://doi.org/https://doi.org/10.1016/S0928-0987(01)00095-1.

[75] Wu IY, Bala S, Škalko-Basnet N, di Cagno MP. Interpreting non-linear drug diffusion data: Utilizing Korsmeyer-Peppas model to study drug release from liposomes. European Journal of Pharmaceutical Sciences 2019;138:105026. https://doi.org/10.1016/j.ejps.2019.105026.

[76] Chen YC, Chen YH. Thermo and pH-responsive methylcellulose and hydroxypropyl hydrogels containing K2SO4 for water retention and a controlled-release water-soluble fertilizer. Science of the Total Environment 2019;655:958–67. https://doi.org/10.1016/j.scitotenv.2018.11.264.

[77] Scaffaro R, Morreale M, lo Re G, la Mantia FP. Degradation of Mater-Bi®/wood flour biocomposites in active sewage sludge. Polymer Degradation and Stability 2009;94:1220–9. https://doi.org/10.1016/j.polymdegradstab.2009.04.028.

Figures

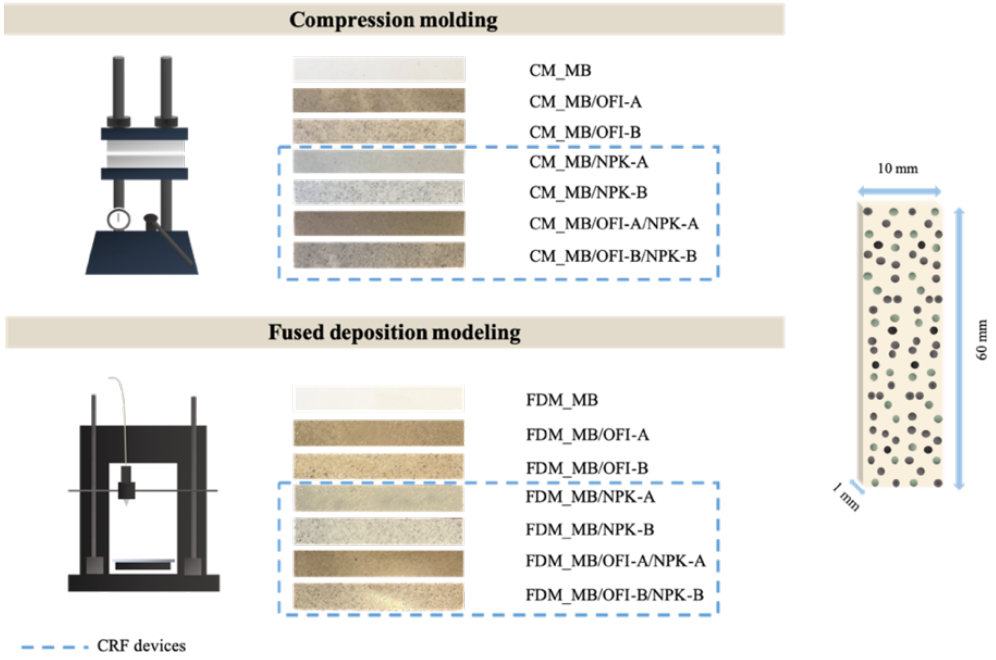

Figure 1 FDM- and CM-obtained samples (photo) and their dimensions. CRF composites have been highlighted with dashed rectangles.

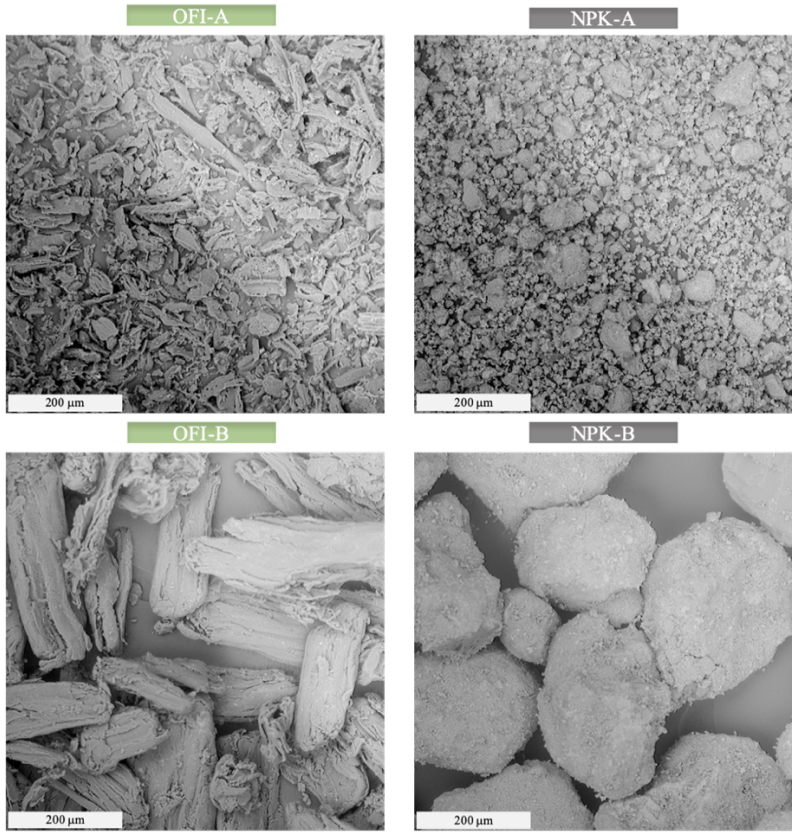

Figure 2 SEM micrograph of OFI and NPK particles (A < 75 µm, B = 75–300 µm).

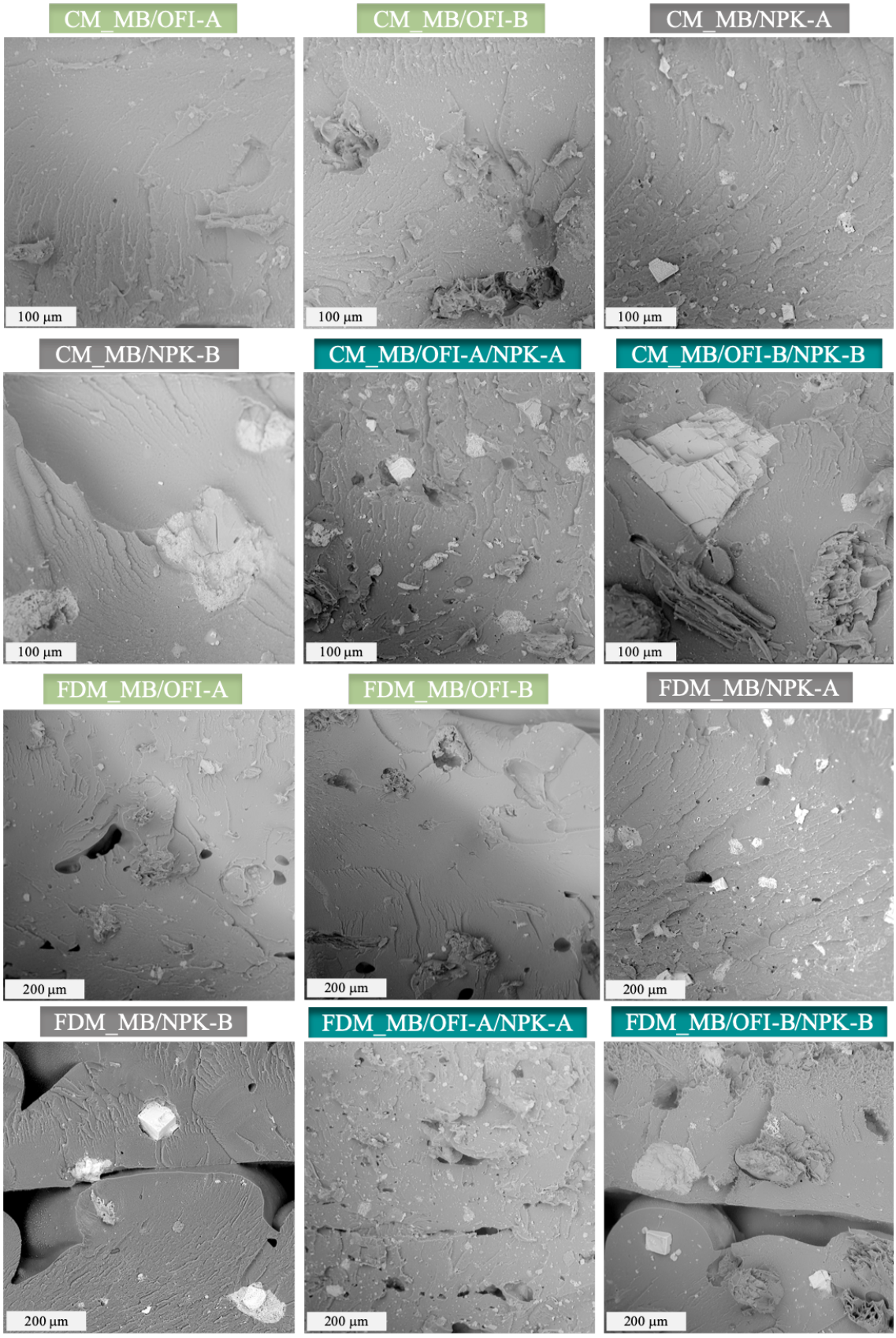

Figure 3 SEM micrograph of fractured cross-section of green composites and CRF devices fabricated for compression molding and FDM.

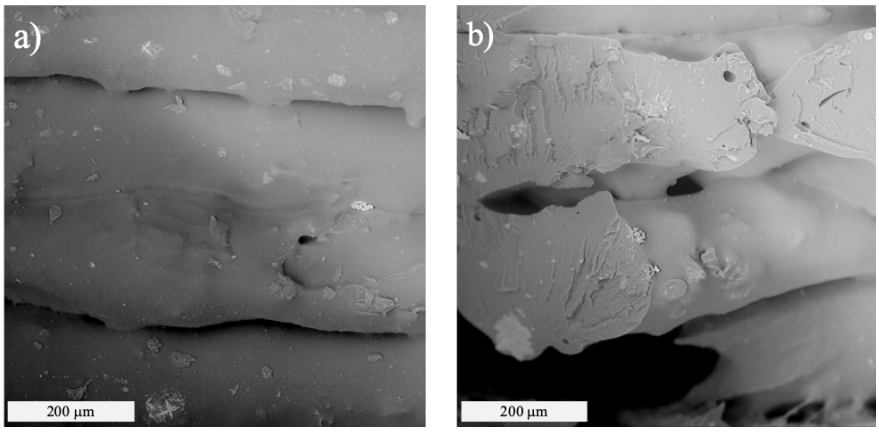

Figure 4 SEM micrograph of adhesion between layers (a) and porous structure (b) of FDM samples.

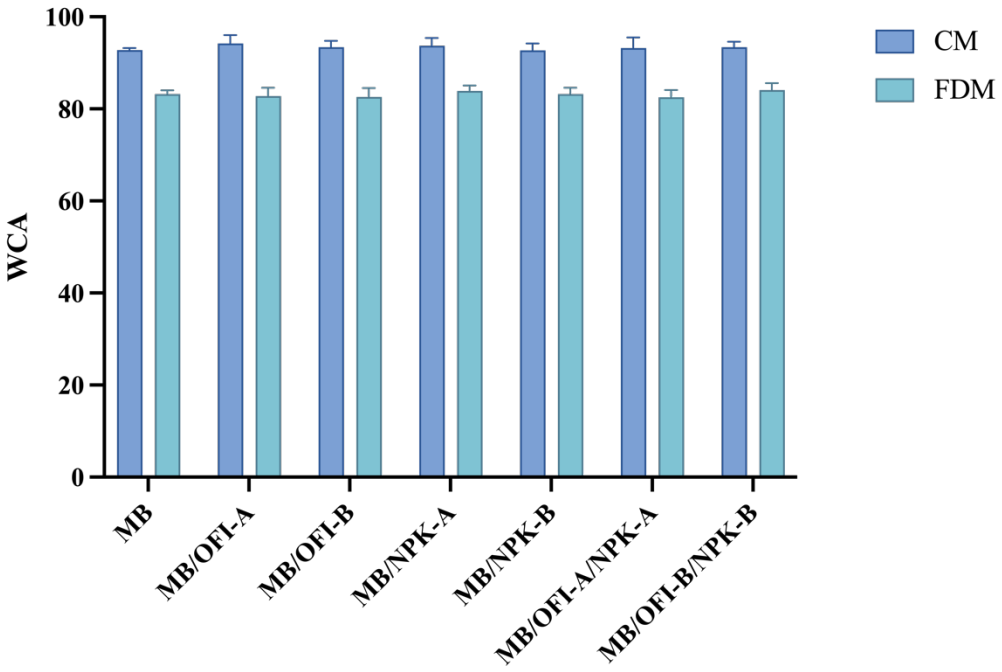

Figure 5 WCA values of compression molded and FDM samples.

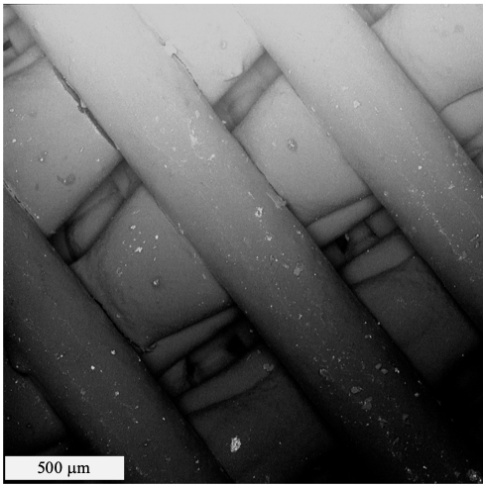

Figure 6 SEM micrograph of FDM composite porous structure, plan view.

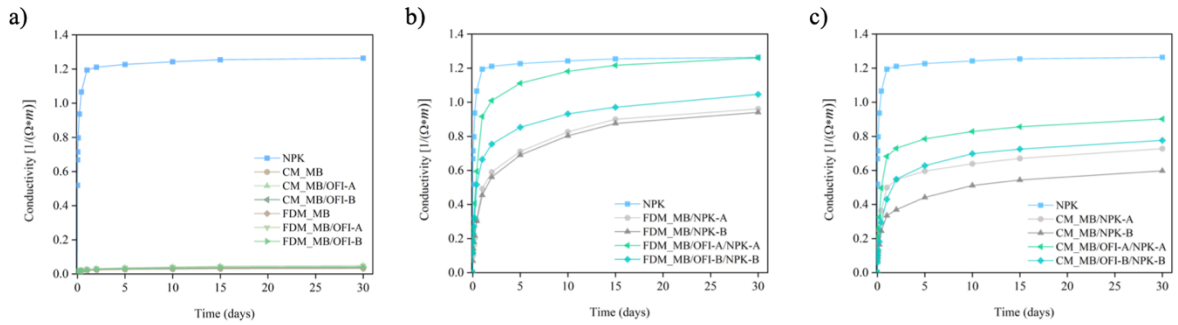

Figure 7 Fertilizer release monitoring by conductivity measurements as function of time for free NPK (reported in each graph for comparison), composites without NPK (a), FDM CRF devices (b) and compression molded CRF devices (c).

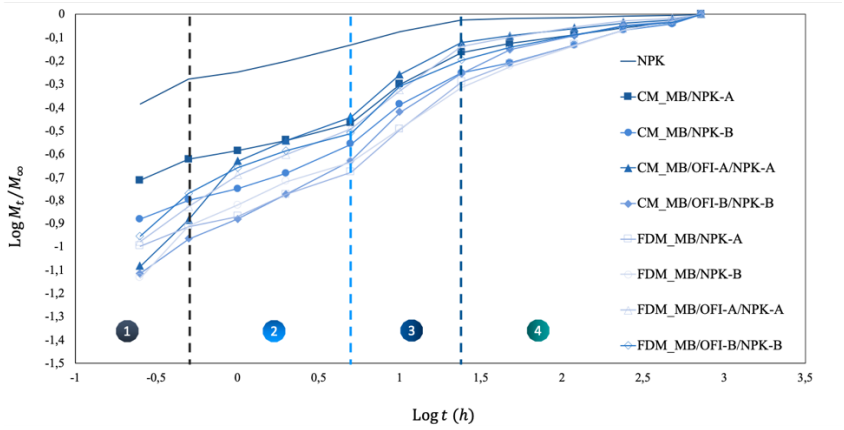

Figure 8 Logarithmic plot of the release data expressed as M_t/M_∞ as function of time for free NPK and CRF devices. Vertical lines and numbers identify different regions of fertilizer release mechanism.

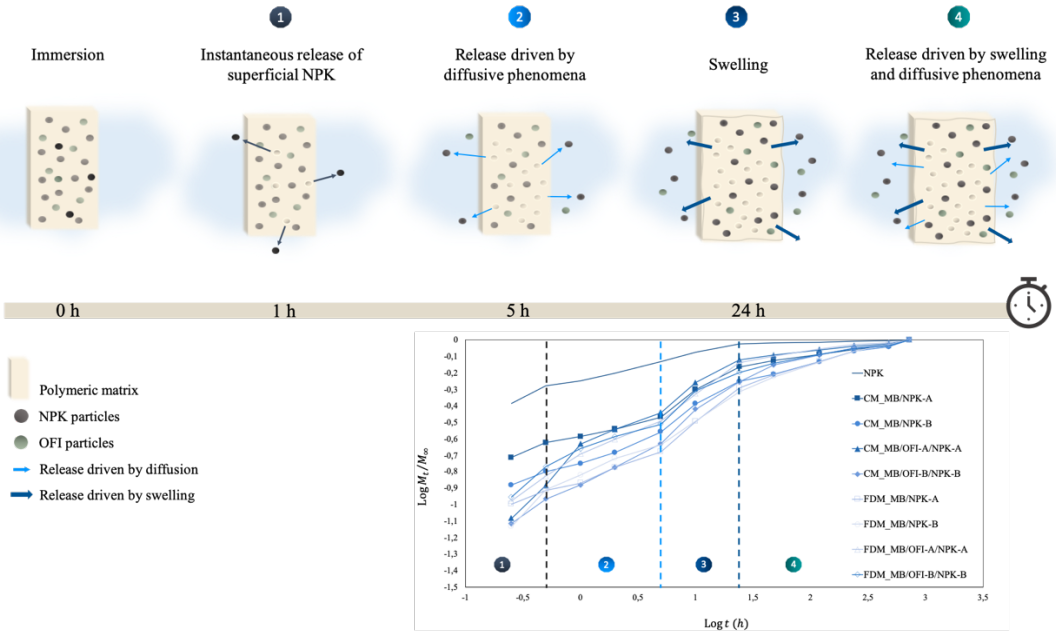

Figure 9 Pictorial description of NPK release mechanism.

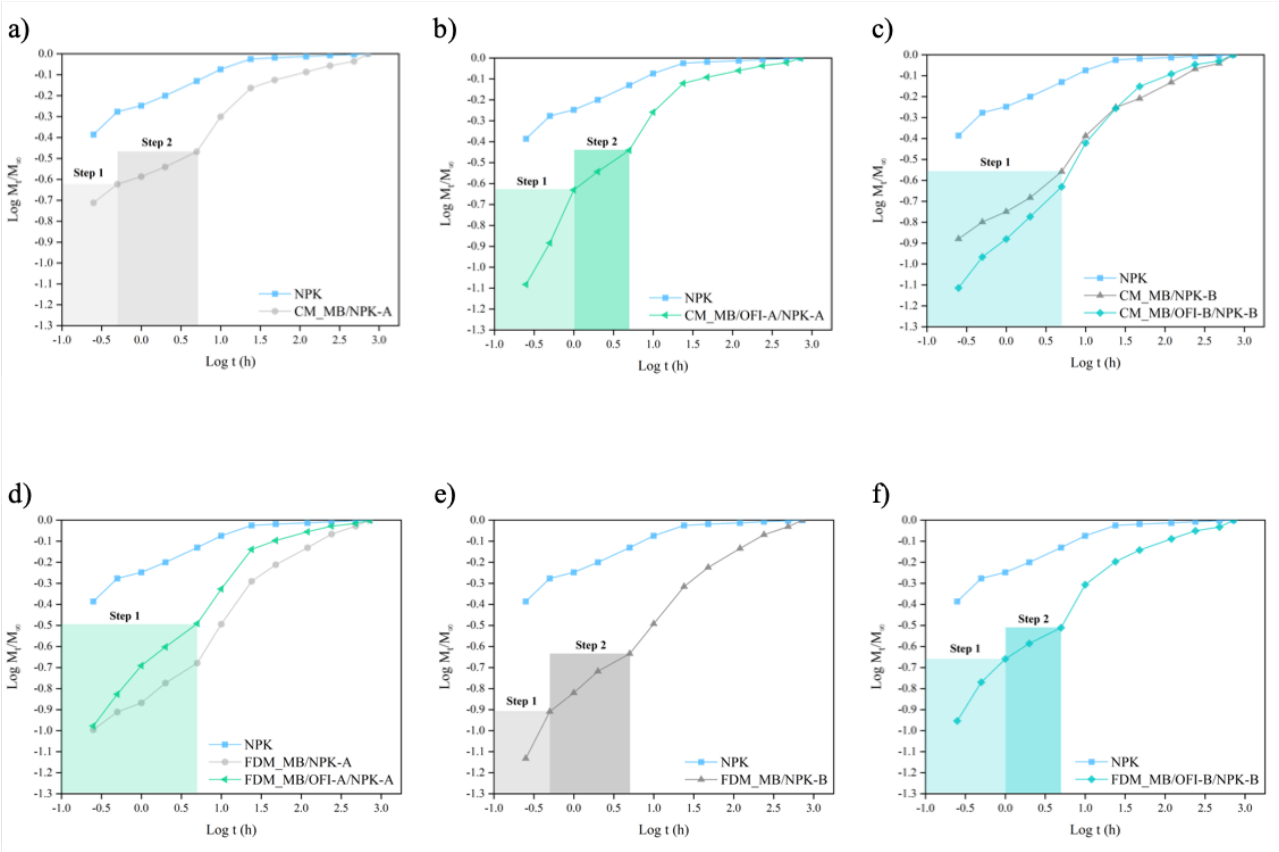

Figure 10 Logarithmic plots of power law model applied to the release data collected in the burst region ($M_t/M_\infty < 0.6$, highlighted by colored portion of the plot) for CM_MB/NPK-A (a); CM_MB/OFI-A/NPK-A (b); CM_MB/NPK-B and CM_MB/OFI-B/NPK-B (c); FDM_MB/NPK-A and FDM_MB/OFI-A/NPK-A (d); FDM_MB/NPK-B (e); FDM_MB/OFI-B/NPK-B (f).

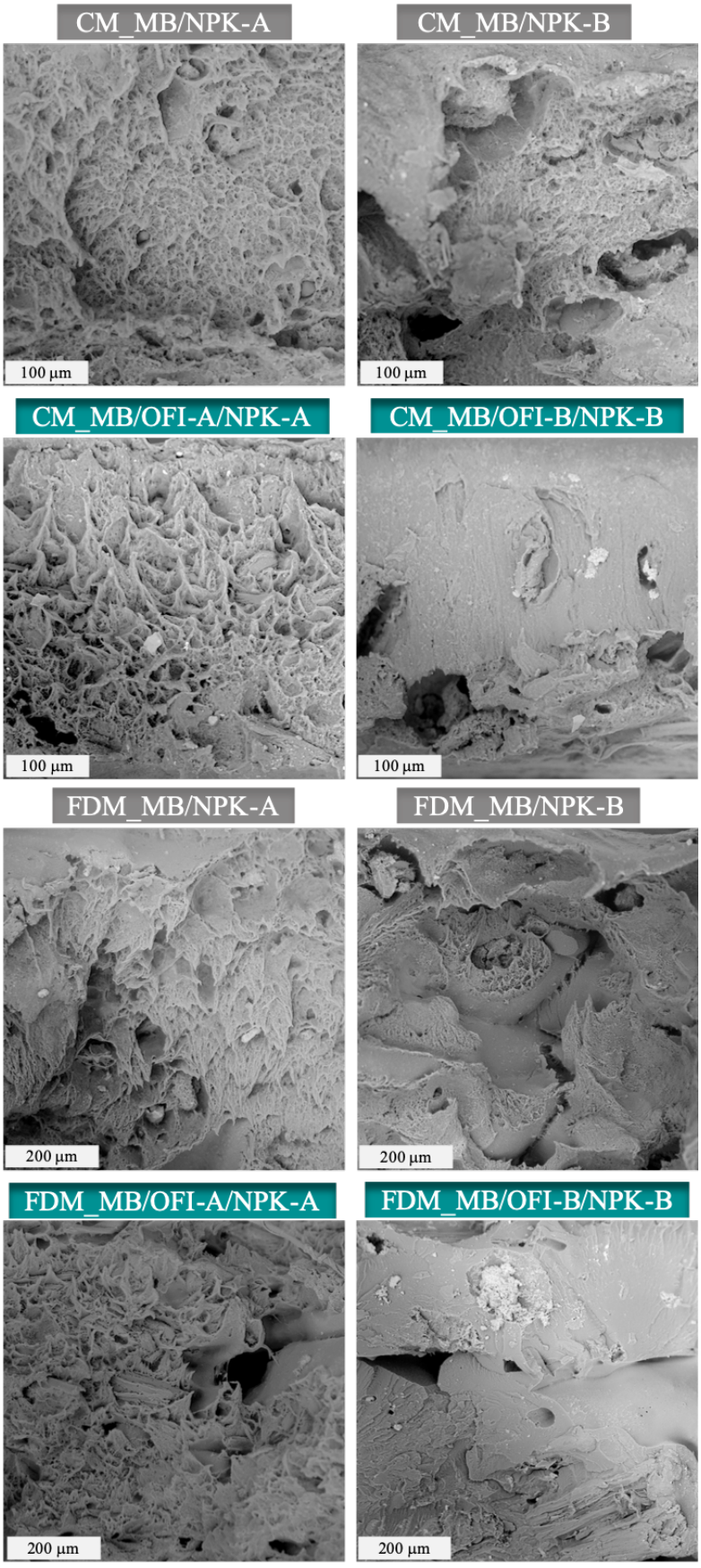

Figure 11 SEM micrograph of fractured cross-section of CRF devices, fabricated for both compression molding and FDM, after soaking in water for 30 days.

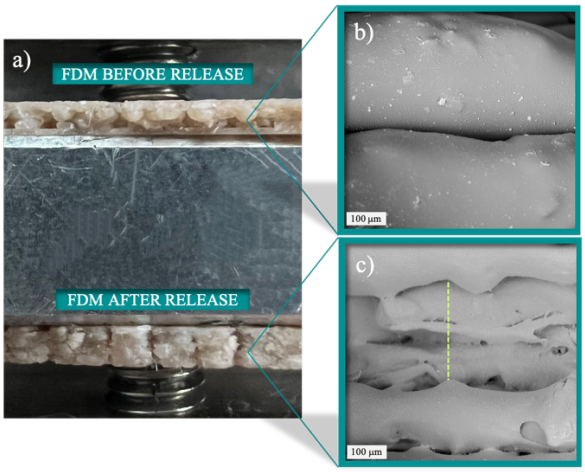

Figure 12 Optical image (a) and SEM micrograph of good adhesion between layers in FDM samples before NPK release (b) and layers detachment in FDM samples after soaking in water for 30 days due to occurrence of swelling (c).

Tables

Table 1 FDM process parameters.

FDM Operating Parameter	**Value**
Nozzle temperature	160 °C
Bed temperature	60 °C
Infill rate	100%
Infill pattern	Rectilinear
Raster angle	± 45°
Layer thickness	0.1 mm
Extrusion width	0.4 mm
Printing speed	50 mm/s
Perimeter shells	1
Sample Orientation	flat

Table 2 Formulation and production technique of investigated samples.

Sample code name	MB content (wt%)	OFI content (wt%)	OFI Mesh size (µm)	NPK content (wt%)	NPK Mesh size (µm)	Production technique
CM_MB	100	0	-	0	-	CM
CM_MB/OFI-A	90	10	< 75	0	-	CM
CM_MB/OFI-B	90	10	300 < 75	0	-	CM
CM_MB/NPK-A	90	0	-	10	< 75	CM
CM_MB/NPK-B	90	0	-	10	300 < 75	CM
CM_MB/OFI-A/NPK-A	80	10	< 75	10	< 75	CM
CM_MB/OFI-B/NPK-B	80	10	300 < 75	10	300 < 75	CM
FDM_MB	100	0	-	0	-	FDM
FDM_MB/OFI-A	90	10	< 75	0	-	FDM
FDM_MB/OFI-B	90	10	300 < 75	0	-	FDM
FDM_MB/NPK-A	90	0	-	10	< 75	FDM
FDM_MB/NPK-B	90	0	-	10	300 < 75	FDM
FDM_MB/OFI-A/NPK-A	80	10	< 75	10	< 75	FDM
FDM_MB/OFI-B/NPK-B	80	10	300 < 75	10	300 < 75	FDM

Table 3 Elastic modulus (E), tensile strength (TS), and elongation at break (EB) of sample obtained by compression molding and FDM.

Sample code name	E (MPa)	TS (MPa)	EB (%)
CM_MB	74.3 ± 1.2	19 ± 0.1	821 ± 0.5
CM_MB/OFI-A	98.1 ± 11	17 ± 0.3	49 ± 0.9
CM_MB/OFI-B	112 ± 8.5	16 ± 0.3	38 ± 1.8
CM_MB/NPK-A	95 ± 1.4	15 ± 1.2	65 ± 2.3

CM_MB/NPK-B	96 ± 1.5	16 ± 0.1	63 ± 2.5
CM_MB/OFI-A/NPK-A	151 ± 7.7	17 ± 0.1	30 ± 0.0
CM_MB/OFI-B/NPK-B	155 ± 8.1	16 ± 0.3	26 ± 1.0
FDM_MB	89 ± 1.3	20 ± 0.2	49 ± 0.8
FDM_MB/OFI-A	113 ± 1.6	17 ± 0.8	21 ± 0.6
FDM_MB/OFI-B	128 ± 1.5	18 ± 1.5	30 ± 1.5
FDM_MB/NPK-A	116 ± 1.6	19 ± 1.7	33 ± 1.3
FDM_MB/NPK-B	120 ± 1.2	20 ± 0.6	49 ± 1.4
FDM_MB/OFI-A/NPK-A	168 ± 1.4	17 ± 1.3	26 ± 1.5
FDM_MB/OFI-B/NPK-B	162 ± 1.8	15 ± 1.5	23 ± 0.1

Table 4 Total amount of NPK released after 30 days.

Sample code name	**NPK released [%]**	
	CM	**FDM**
MB/NPK-A	58	76
MB/NPK-B	47	74
MB/OFI-A/NPK-A	71	100
MB/OFI-B/NPK-B	61	83

Table 5 Values of slopes (n) and intercepts (k) of fitting of Peppas-Korsmeyer model power law applied to the release data collected in the burst region ($M_t / M_\infty < 0.6$).

Sample code name	Step 1		Step 2	
	K	n	K	n
CM_MB/NPK-A	1.96	0.30	1.83	0.16
CM_MB/NPK-B	1.52	0.25	-	-
CM_MB/OFI-A/NPK-A	1.71	0.78	1.72	0.27
CM_MB/OFI-B/NPK-B	1.36	0.35	-	-
FDM_MB/NPK-A	1.38	0.24	-	-
FDM _MB/NPK-B	1.61	0.74	1.42	0.27
FDM _MB/OFI-A/NPK-A	1.55	0.34	-	-
FDM _MB/OFI-B/NPK-B	1.67	0.46	1.67	0.21

Table 6 Elastic modulus (E), tensile strength (TS), and elongation at break (EB) of sample obtained by compression molding and FDM after NKP release.

Sample code name	E (MPa)	TS (MPa)	EB (%)
CM_MB	128 ± 1.6	6.1 ± 1.8	7.3 ± 2.1
CM_MB/OFI-A	135 ± 11	5.4 ± 0.0	8.9 ± 1.6
CM_MB/OFI-B	150 ± 3.1	5.7 ± 0.8	6.4 ± 0.4
CM_MB/NPK-A	94.6 ± 0.8	5.3 ± 0.6	8.4 ± 0.0
CM_MB/NPK-B	95.4 ± 3.7	5.7 ± 0.4	7.8 ± 0.8
CM_MB/OFI-A/NPK-A	137 ± 3.9	6.3 ± 0.3	7.5 ± 0.4
CM_MB/OFI-B/NPK-B	143 ± 9.5	4.8 ± 2.2	4.7 ± 2.0
FDM_MB	85.6 ± 1.1	5.9 ± 0.6	13 ± 1.4
FDM_MB/OFI-A	101 ± 1.7	5.2 ± 0.4	7.8 ± 1.4
FDM_MB/OFI-B	114 ± 0.5	5.6 ± 1.7	7.4 ± 0.7
FDM_MB/NPK-A	90.7 ± 1.5	5.9 ± 1.3	8.9 ± 1.3
FDM_MB/NPK-B	101 ± 0.7	6.1 ± 0.2	8.4 ± 0.3
FDM_MB/OFI-A/NPK-A	105 ± 0.4	5.9 ± 1.5	8.9 ± 0.8

FDM_MB/OFI-B/NPK-B	104 ± 1.4	5.7 ± 1.2	8.4 ± 1.6

Data Availability Statement: The data presented in this study are available on request from the corresponding authors.

Funding statement: This research did not receive any specific grant from funding agencies in the public, commercial, or not-for-profit sectors.

Conflict of interest disclosure: The authors declare no conflict of interest.